



Lens dose reduction with a bismuth shield in neuro cone-beam computed tomography: an investigation on optimum shield device placement conditions

Satoru Kawauchi^{1,2,3} · Koichi Chida² · Yusuke Hamada¹ · Wataro Tsuruta⁴

Received: 15 July 2021 / Revised: 8 November 2021 / Accepted: 9 November 2021 / Published online: 18 November 2021
© Japanese Society of Radiological Technology and Japan Society of Medical Physics 2021

Abstract

This study aimed to determine the placement distance, number, and position of the bismuth shield for developing a lens protective device for cone-beam computed tomography (CBCT). To determine the dose reduction rate, the lens doses were measured using an anthropomorphic head phantom and a real-time dosimeter. The image quality assessment was determined by analyzing the change in the pixel value, caused by the bismuth shield, and the artifact index was calculated from the pixel value and image noise within various regions of interest in the head phantom. When the distance between the bismuth shield and the subject was increased, the image quality deteriorated less, but there was also a decrease in the lens dose reduction rate. Upon changing the number of bismuth shields from 1-ply to 2-ply, the dose reduction rate increased; however, there was a decrease in the image quality. Additionally, placing the bismuth shield outside of the subject improved the dose reduction rate without deteriorating the image quality. The optimum placement conditions of the bismuth shield were concluded as follows: positioned outside, placed 10 mm from the surface of the subject, and used a 1-ply bismuth shield. When these placement conditions were used, the lens dose reduction rate was $26.9 \pm 0.36\%$ (right–left average) for the “bismuth shield: separate”. The protective device developed in this study will contribute to radiation dose reduction in CBCT scans.

Keywords Cone-beam CT (CBCT) · Interventional neuroradiology (INR) · Lens dose · Radioprotection · Bismuth shield · Image quality

1 Introduction

The use of interventional radiology procedures such as percutaneous coronary intervention and cerebral angiography are increasing because of its non-invasiveness compared to surgeries. However, the radiation dose during these procedures is high [1–9]. For example, cone-beam CT (CBCT) scans performed with an angiographic unit during diagnostic cerebral angiography and interventional neuroradiography (INR) result in a high radiation dose to the patient. This also affects the lens of the eye, since it is one of the most radiosensitive tissues of the human body. Therefore, it is essential to evaluate the lens dose for each individual during angiography [10].

For cerebral angiography, the total radiation exposure for patients is roughly divided into fluoroscopy, digital subtraction angiography (DSA), 3-dimensional rotational angiography, CBCT, and other imaging. In the past, fluoroscopy and DSA were the main contributors to total patient exposure. However, the contribution of CBCT has increased with the

✉ Satoru Kawauchi
shibaken.shatle@kjd.biglobe.ne.jp

Koichi Chida
chida@med.tohoku.ac.jp

Yusuke Hamada
yusuke71640@yahoo.co.jp

Wataro Tsuruta
wataro@cf6.so-net.ne.jp

¹ Department of Radiology, Toranomon Hospital, 2-2-2 Toranomon, Minato-ku, Tokyo 105-8470, Japan

² Department of Radiological Technology, Tohoku University Graduate School of Medicine, 2-1 Seiryō, Aoba-ku, Sendai, Miyagi 980-8575, Japan

³ Okinaka Memorial Institute for Medical Research, 2-2-2 Toranomon, Minato-ku, Tokyo 105-8470, Japan

⁴ Department of Endovascular Neurosurgery, Toranomon Hospital, 2-2-2 Toranomon, Minato-ku, Tokyo 105-8470, Japan

advances in angiography units in recent years. In a previous study, approximately 25% of the total radiation exposure of the eye lens of a patient was induced using CBCT [11].

The lens dose per procedure cannot be ignored, since the number of CBCT scans has increased because of reports of improvement in image quality and clinical benefits [12–15]. In the International Commission on Radiological Protection (ICRP) Publication 118, the threshold value for the absorbed dose to the lens was described as 0.5 Gy [16–19]. This report indicates that repeated CBCT scans may have deterministic effects on the eye lens, including the risk of cataracts. Thus, it is important to estimate and reduce the radiation dose of CBCT [11, 20].

The lens doses associated with CBCT were reported as 16.0–32.4 mGy in a previous study [10, 11, 20]. In INR, several new devices such as intracranial stents and flow diverter stents have emerged, which have substantially improved the procedure for cerebral aneurysm embolization and the treatment of large or giant cerebral aneurysms [21]. Several diseases that were previously contraindicated for treatment are now being treated using INR. However, while good clinical outcomes were achieved, the radiation dose to the patient was also increased, as the procedure became more sophisticated and complex. In cerebral angiography, treatment indications are often determined based on the results of diagnostic cerebral angiography, and INR is performed. Repeated angiography or INR is also performed in cases of disease recurrence, which results in an accumulation of radiation dose, even if the threshold dose has not exceeded during a single procedure. Thus, appropriate radiation protection measures are required for each procedure, including CBCT.

Various studies have reported that tube current modulation (TCM), organ-based TCM (OB-TCM), gantry tilt, and shield methods protect lenses in head CT scans [22–31]. In a neuro-CBCT scan, the tube voltage, tube current, additional filter, and scanning method are part of a fixed protocol. Therefore, the TCM, OB-TCM, and gantry tilt methods cannot be used to reduce the lens dose in CBCT. Consequently, the only method to protect the lens is the shield method.

In a previous study, suitable protective materials for lenses used in CBCT were investigated based on the dose reduction rate and image quality [32]. We found that bismuth shields and lead goggles are suitable protective materials. Furthermore, by dividing the bismuth shield into two parts according to the positions of the right and left lenses, the image quality was improved without changing the dose reduction rates (approximately 14.4%). Although the use of protective materials such as bismuth shields is a useful method for reducing the lens dose, there is still room for improvement in the dose reduction rate and image quality. Among previous studies on bismuth shields for head CT scans, only a few have reported on the distance between the surface of the object and the bismuth shield and the

number of bismuth shields [24, 25, 30, 31, 33]. Raissaki et al. investigated the use of a bismuth shield for pediatric head CT scans and reported that a 10-mm gap between the bismuth shield and the surface of the eyes was recommended [30]. Although increasing the distance of the bismuth shield is useful in preventing deterioration of image quality, the appropriate placement distance may differ between pediatric head CT and adult head CBCT, because the rotation orbits of the X-ray tube and the head size of the patients are different. To our knowledge, for CBCT scans performed during cerebral angiography and INR, there is no previous study which assessed the bismuth placement conditions, such as the distance between the surface of the subject and the bismuth shield, the number of bismuth shields, and the placement position of the bismuth shield.

The aim of this study is to determine the suitable placement conditions for bismuth shields using head phantoms, to optimize dose reduction and image quality in CBCT.

2 Materials and methods

2.1 Scanning technique

This study was performed using a biplane X-ray device (Azurion7 B20/15; Philips Healthcare, Best, The Netherlands) equipped with flat-panel detectors. An anthropomorphic adult head phantom (PH-3; Kyoto Kagaku Co., Ltd., Kyoto, Japan) was scanned using a whole-brain CBCT protocol (Table 1). All parameters for the CBCT scan were constant and were not changed by a radiological technologist. The CBCT scan was performed by rotating the arc from the left anterior oblique 120° to the right anterior oblique 120° around the posterior aspect of the head phantom (Fig. 1).

Table 1 Scan parameters for the CBCT scan and reconstruction

Tube voltage	120 kVp
Tube current	250 mA
Additional filter	0.4 mm Al + 1.0 mm Cu
Pulse width	5 ms
Rotation angle	240 degree
Frame rate	30 frame/sec
Source-to-detector distance	120 cm
Scan time	20.8 s
Detector size	28.8 × 38.4 cm (48.0 cm diagonal)
Focal spot size	0.7 mm
Number of images	622
Reconstruction kernel	Exam preset
Number of pixels	384

Fig. 1 Rotational orbit of the X-ray tube for the cone-beam computed tomography (CBCT) scan. CBCT is performed by rotating the arc from the left anterior oblique 120° to the right anterior oblique 120° around the posterior aspect of the head phantom

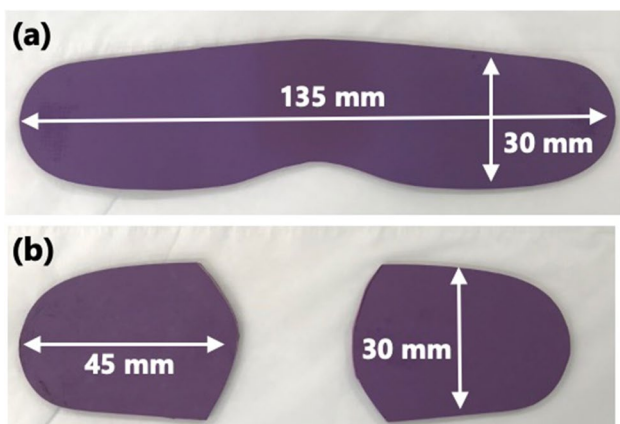
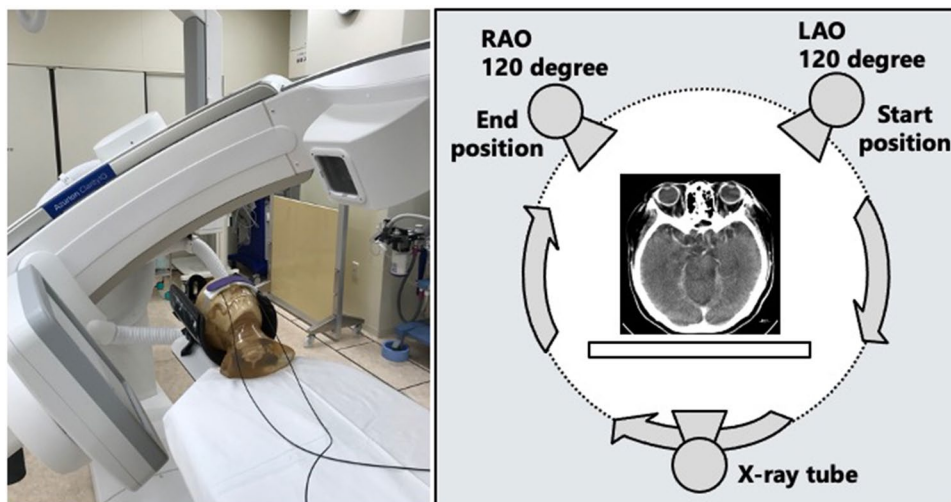


Fig. 2 Two types of bismuth shield: **a** Bismuth shield: eye mask (long axis: 135 mm, short axis: 30 mm). **b** Bismuth shield: separate (long axis: 45 mm, short axis: 30 mm)

2.2 Bismuth shield devices for eye protection

A commercially available bismuth shield (CT eye shield, 0.06 mm Pb equivalent; FLAIR Co., Ltd, Tokyo, Japan) was used in this study. Two types of bismuth shields with different shapes, “eye mask” and “separate” (denoted as “bismuth shield: eye mask” and “bismuth shield: separate”), were prepared, as reported in a previous study [32] (Fig. 2). “Bismuth shield: separate” was designed to cover only the eyeball.

2.3 Change of bismuth placement conditions

CBCT scans were performed using “bismuth shield: eye mask” at varying distances between the surface of the head phantom and bismuth shield, by placing foam pads—from 0 to 20 mm, at every 5 mm (Fig. 3). One and two layers (denoted as “1-ply” and “2-ply”) of “bismuth shield: eye mask” and “bismuth shield: separate” were placed over the

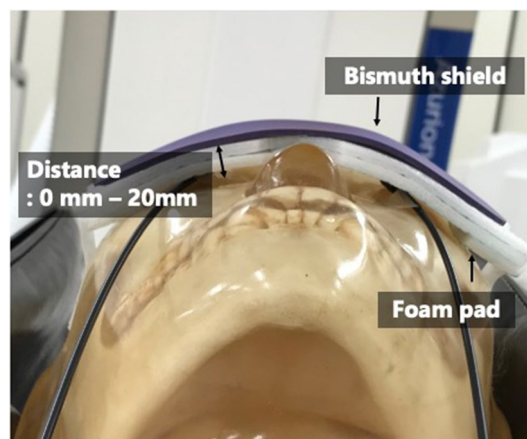


Fig. 3 Photograph of head phantom when various CBCT scans were obtained at the distances between the surface of the head phantom and bismuth shield

eyes of the head phantom (Fig. 4). To evaluate the position dependence of the bismuth shield, the position just above the eyeball of the head phantom was defined as “middle.” “Bismuth shield: separate” was placed 17 mm toward the eye, defined as “inside,” and 17 mm away from the eye, defined as “outside.” The positions corresponding to the lenses were barely covered by protective materials (Fig. 5). Each CBCT scan was performed three times.

2.4 Lens dose measurement with bismuth shield

A real-time dosimeter (RD-1000, Toreck Co., Ltd; Yokohama, Japan) was used to measure the doses of the right and left lenses. The dosimeter was equipped with a Y₂O₂S: Eu, Sm phosphor for the sensor, and a plastic optical fiber for the cable. The shape of the sensor was cylindrical with a length of 1.2 mm and a diameter of 1.4 mm. The sensors

Fig. 4 Radiograph of the head phantom for the different numbers of the bismuth shield. **a** 1-ply bismuth shield and **b** 2-ply bismuth shield.

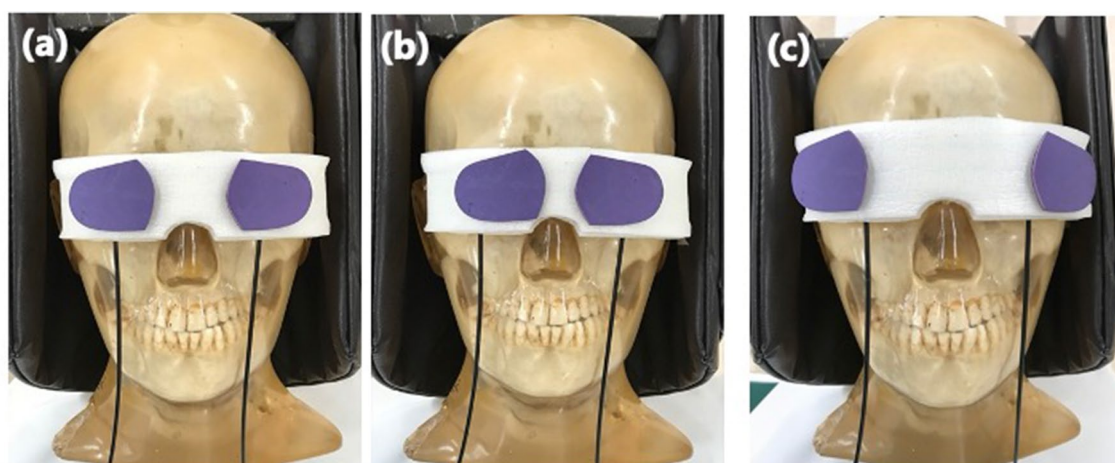
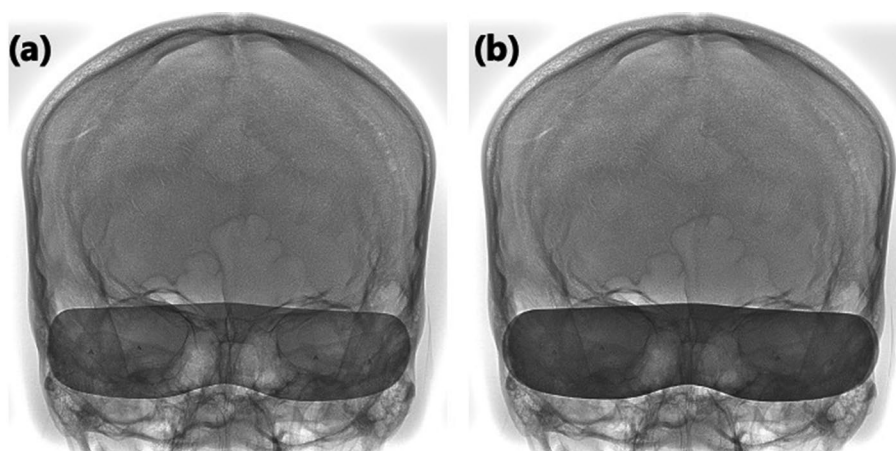


Fig. 5 Photograph of the head phantom at different positions of “bismuth shield: separate.” **a** Middle, **b** inside, and **c** outside.

were placed at positions corresponding to the right and left lens surfaces of the head phantom (Fig. 6).

In a previous study, the real-time dosimeter demonstrated good fundamental characteristics related to dose and dose rate dependence [34–40]. However, the entrance surface doses (air kerma) obtained from the real-time dosimeter have been reported to be underestimated relative to the calibrated radio-photoluminescence glass dosimeters (RPLDs) [38]. To measure entrance surface dose with high accuracy, it was necessary to correct the measured value of the real-time dosimeter using the calibration factor obtained from the calibrated RPLDs. Kato et al. measured the radiation doses for 40 clinical cases who underwent radiofrequency catheter ablation using a real-time dosimeter and RPLDs in the same area of the chest. The resultant calibration factor used for converting the measured value of the RPLD to the entrance surface dose of the real-time dosimeter was 1.15 [38]. Furthermore, the entrance surface dose was converted to the absorbed lens dose by multiplying the mass energy

absorption coefficient ratio for the lens to air ($= 1.08$). To evaluate the protective effect of the bismuth shields, the dose reduction rate was calculated using the following equation:

$$\text{Dose reduction rate [\%]} = \left(1 - \left(\frac{\text{Lens dose with bismuth shield}}{\text{Lens dose for the reference scan}} \right) \right) \times 100$$

The lens doses and dose reduction rates are presented as mean \pm standard deviation.

2.5 Quantitative image analysis with bismuth shield

Image quality was evaluated by measuring the pixel value, noise, and artifact index (AI) of the head phantom. Using a Ziostation2 workstation (Ziosoft, Inc., Tokyo, Japan), the pixel values and image noises were acquired based on a circular region of interest (ROI) with a diameter of 50 mm for

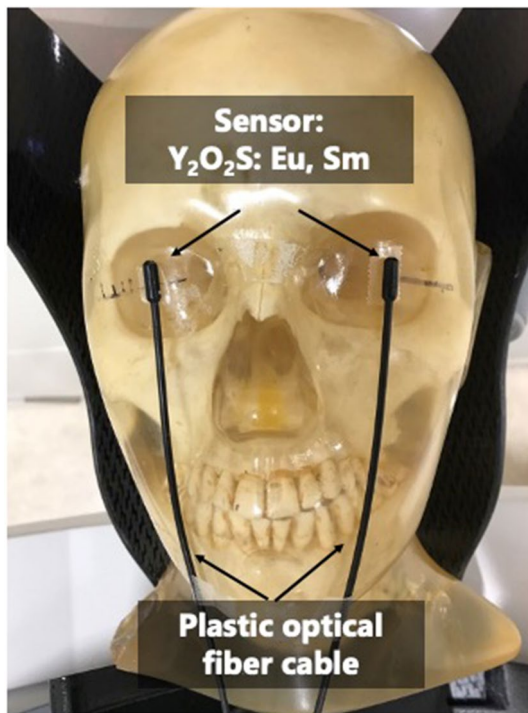


Fig. 6 Real-time dosimeters were placed on the lens surfaces of the anthropomorphic head phantom

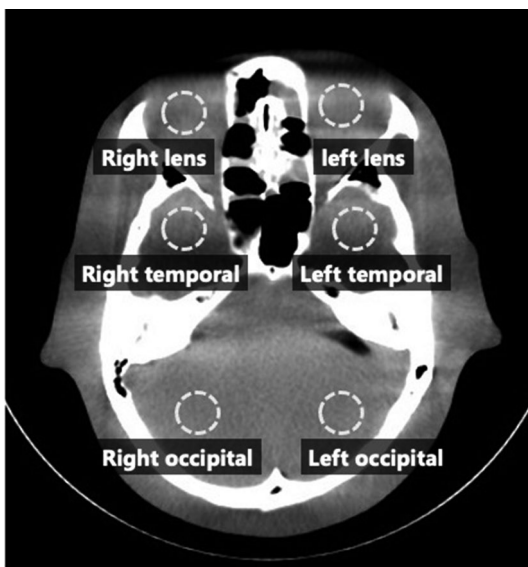


Fig. 7 Image of the six regions of interest used to measure the pixel value and noise of the head phantom

six regions (right lens, left lens, right temporal, left temporal, right occipital, and left occipital, as shown in Fig. 7). These regions were selected to investigate the effect of bismuth shield placement on the depth direction of the head

(anterior → posterior direction). The change in the pixel value caused by the bismuth shield was expressed as ΔPV

$$\Delta PV = PV_{\text{bismuth}} - PV_{\text{reference}}$$

PV_{bismuth} : pixel value with bismuth shield.

$PV_{\text{reference}}$: pixel value of reference scan.

Noise was defined as the standard deviation of pixel values in the ROI. The AIs of the regions of the head phantom, which is an index for evaluating streak artifacts, were defined as follows [41–43]:

$$AI = \sqrt{(\text{Noise}_{\text{bismuth}})^2 - (\text{Noise}_{\text{reference}})^2}$$

$\text{Noise}_{\text{bismuth}}$: noise with bismuth shield.

$\text{Noise}_{\text{reference}}$: noise of reference scan.

The ΔPV s and AIs of each region were calculated based on the ROIs placed in the six regions, as shown in Fig. 7. The ΔPV s and AIs are presented as mean \pm standard deviation.

3 Results

3.1 Lens dose measurement and image quality assessment with a change of distance

Table 2 presents the right, left, and average lens doses and dose reduction rates of the head phantom at varying distances from the eye surface. The representative average lens dose was 30.9 ± 0.11 mGy for the reference scan, and 20.1 ± 0.14 mGy, 26.5 ± 0.12 mGy, and 31.3 ± 0.09 mGy for distances of 0, 10, and 20 mm, respectively.

The representative average dose reduction rates were $34.8 \pm 0.62\%$, $14.3 \pm 0.51\%$, and $-1.4 \pm 0.48\%$ for distances of 0, 10, and 20 mm, respectively.

Images of the head phantom at different distances from the eye surface are shown in Fig. 8. Figures 9 and 10 show the ΔPV s and AIs for each region of the head phantom at different distances when the “bismuth shield: eye mask” was used. The ΔPV s in the right and left lens regions decreased with an increase in the distance of the bismuth shield. AIs excluding the right and left occipital regions also decreased with the increasing distance.

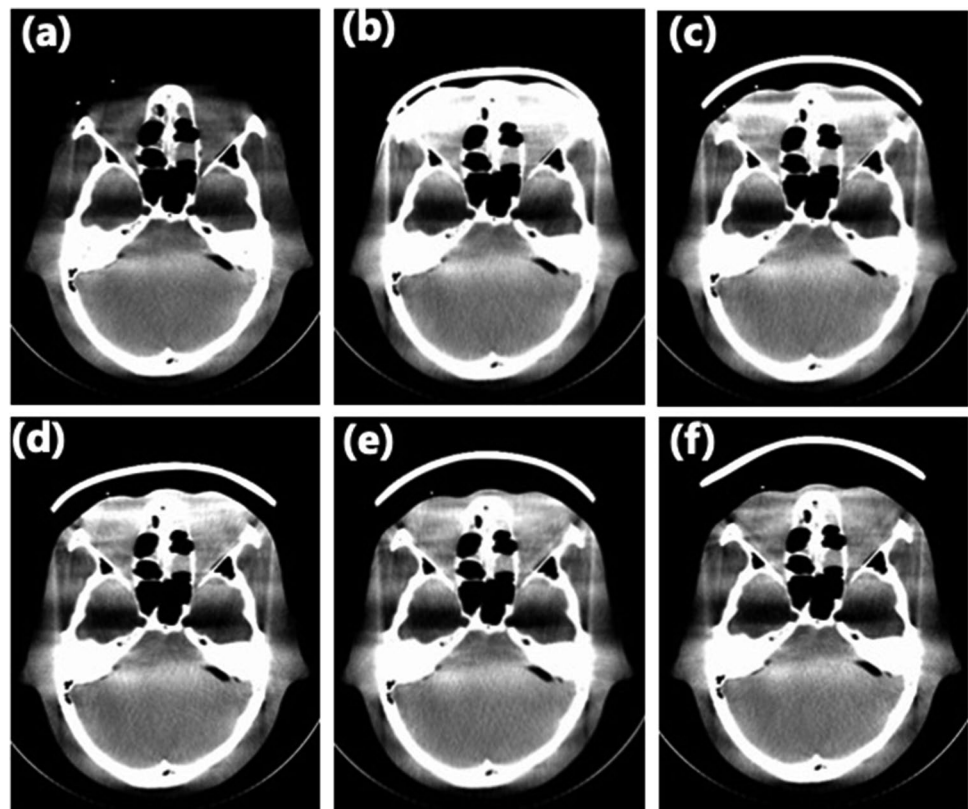
3.2 Lens dose measurement and image quality assessment with different numbers of bismuth shields

Table 3 presents the right, left, and average lens doses and dose reduction rates of the head phantom for varying numbers of bismuth shields. The average lens doses were 26.5 ± 0.12 mGy for 1-ply and 24.7 ± 0.11 mGy for 2-ply

Table 2 Lens doses and lens dose reduction rates for different distances from the surface of the head phantom

	Lens dose [mGy]			Dose reduction rate [%]		
	Right lens	Left lens	Average	Right lens	Left lens	Average
Reference	30.6±0.12	31.2±0.14	30.9±0.11	–	–	–
0 mm	20.0±0.13	20.2±0.14	20.1±0.14	34.5±0.61	35.1±0.63	34.8±0.62
5 mm	24.7±0.14	25.7±0.14	25.2±0.14	19.1±0.55	17.8±0.59	18.5±0.54
10 mm	26.1±0.14	26.9±0.11	26.5±0.12	14.8±0.58	13.9±0.52	14.3±0.51
15 mm	27.4±0.12	28.2±0.18	27.8±0.15	10.5±0.51	9.8±0.71	10.2±0.58
20 mm	30.6±0.07	32.0±0.12	31.3±0.09	–0.12±0.44	–2.7±0.62	–1.4±0.48

Data are presented as mean ± standard deviation

Fig. 8 Images of head phantom at different distances from the eye surface. **a** Reference, **b** 0 mm, **c** 5 mm, **d** 10 mm, **e** 15 mm, and **f** 20 mm.

of “bismuth shield: eye mask.” The average lens doses were 26.3 ± 0.15 mGy for 1-ply and 25.3 ± 0.09 mGy for 2-ply of “bismuth shield: separate.”

The average lens dose reduction rates were $14.3 \pm 0.51\%$ for 1-ply and $20.2 \pm 0.45\%$ for 2-ply of “bismuth shield: eye mask.” The average lens dose reduction rates were $14.8\% \pm 0.58\%$ for 1-ply and $18.1 \pm 0.41\%$ for 2-ply of “bismuth shield: separate.”

Images of the head phantom for varying numbers of bismuth shields are shown in Fig. 11. Figures 12 and 13 show the Δ PVs and AIs for each region of the head phantom for varying numbers of bismuth shields. The Δ PVs in the right and left lens regions were markedly increased when 2-ply of “bismuth shield: eye mask “ and “bismuth shield: separate”

were used. The AIs, excluding the right and left occipital regions, also increased with an increase in the number of bismuth shields.

3.3 Lens dose measurement and image quality assessment with a change of position

Table 4 presents the right, left, and average lens doses and lens dose reduction rates of the head phantom for the different positions of the bismuth shield. The average lens doses were 31.4 ± 0.24 mGy for the inside position, 26.3 ± 0.15 mGy for the middle position, and 22.8 ± 0.07 mGy for the outside position. The average lens

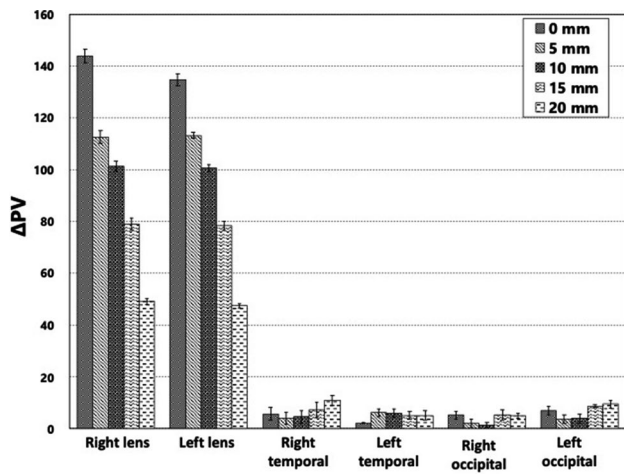


Fig. 9 ΔPVs for different distances from the surface of the head phantom for each ROI. Error bars represent the standard deviation of ΔPV

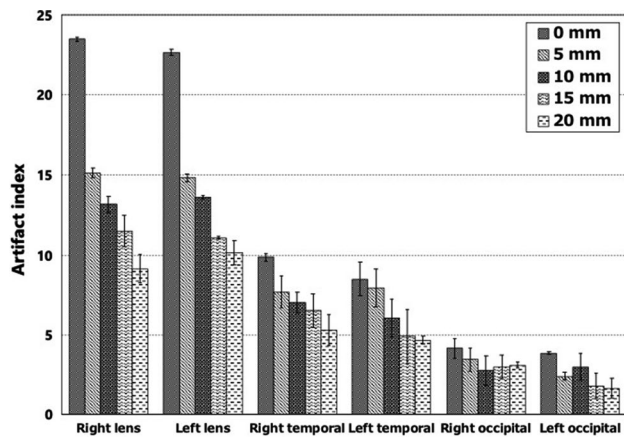


Fig. 10 Artifact indices for different distances from the surface of the head phantom for each region of interest. Error bars represent the standard deviation of the artifact index

dose reduction rates were $-1.8 \pm 0.86\%$ for the inside position, $14.8 \pm 0.58\%$ for the middle position, and $26.9 \pm 0.36\%$ for the outside position.

Table 3 Lens doses and lens dose reduction rates for the different bismuth shield numbers

	Lens dose [mGy]			Dose reduction rate [%]		
	Right lens	Left lens	Average	Right lens	Left lens	Average
Reference	30.6 ± 0.12	31.2 ± 0.14	30.9 ± 0.11	–	–	–
Eye mask: 1-ply	26.1 ± 0.14	26.9 ± 0.11	26.5 ± 0.12	14.8 ± 0.58	13.9 ± 0.52	14.3 ± 0.51
Eye mask: 2-ply	25.0 ± 0.11	24.4 ± 0.11	24.7 ± 0.11	18.3 ± 0.47	22.0 ± 0.50	20.2 ± 0.45
Separate: 1-ply	26.3 ± 0.19	26.3 ± 0.12	26.3 ± 0.15	13.8 ± 0.70	15.7 ± 0.54	14.8 ± 0.58
Separate: 2-ply	25.7 ± 0.11	25.0 ± 0.06	25.3 ± 0.09	16.1 ± 0.49	20.0 ± 0.42	18.1 ± 0.41

The distance between the bismuth shield and the surface of the eyes was 10 mm. Data are presented as mean \pm standard deviation

Images of the head phantom for different positions of the bismuth shield are shown in Fig. 14. Figure 15 shows the ΔPVs for each region of the head phantom for each position of the bismuth shield. The ΔPVs of the lens and temporal regions were slightly decreased when the positions of the “bismuth shield: separate” were changed from the middle to the inside positions. Conversely, although there were almost no changes in the ΔPVs of the lens regions, the ΔPVs of the temporal regions increased with the change in the positions of the “bismuth shield: separate” from the middle to the outside positions.

Figure 16 shows the AIs for each region of the head phantom for each position of the bismuth shield. The AIs of the right and left lens regions were slightly increased when the position of the “bismuth shield: separate” was changed from the middle to the inside and outside positions.

4 Discussion

4.1 Lens dose measurement and image quality assessment with a change of distance

Changes in the lens dose reduction rate and image quality were examined by changing the distance between the surface of the head phantom and the bismuth shield. The results showed that the optimum distance was 10 mm.

Although the lens dose reduction rates increased when the bismuth shields were placed near the surface of the phantom, the ΔPVs and AIs of the right and left lenses increased. This shows that closer the bismuth shield is to the head phantom, the more primary X-rays can be cut.

Conversely, when the bismuth shield was placed farther from the head phantom, the image quality deteriorated less; however, the lens dose reduction rate also decreased. This can be attributed to the increase in the primary X-rays.

When the bismuth shield placement distance was 20 mm from the phantom surface, the average dose reduction rate was $-1.4 \pm 0.48\%$, which resulted in a higher lens dose than when no bismuth shield was placed. This is because there was almost no primary X-ray shielding effect when the

Fig. 11 Images of head phantom for different numbers of bismuth shields. **a** Reference, **b** 1-ply of “bismuth shield: eye mask”, **c** 2-ply of “bismuth shield: eye mask”, **d** 1-ply of “bismuth shield: separate”, and **e** 2-ply of “bismuth shield: separate”

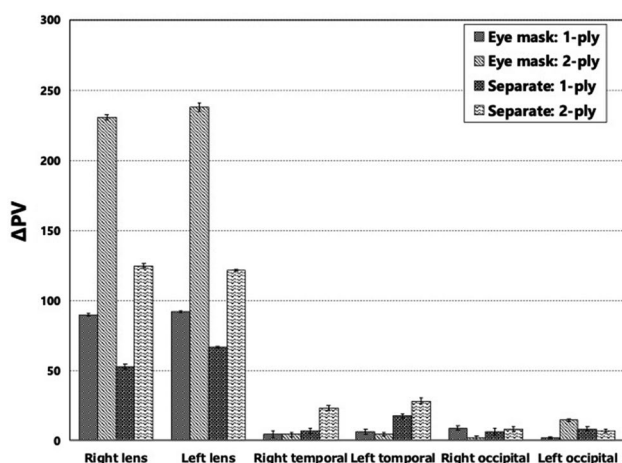
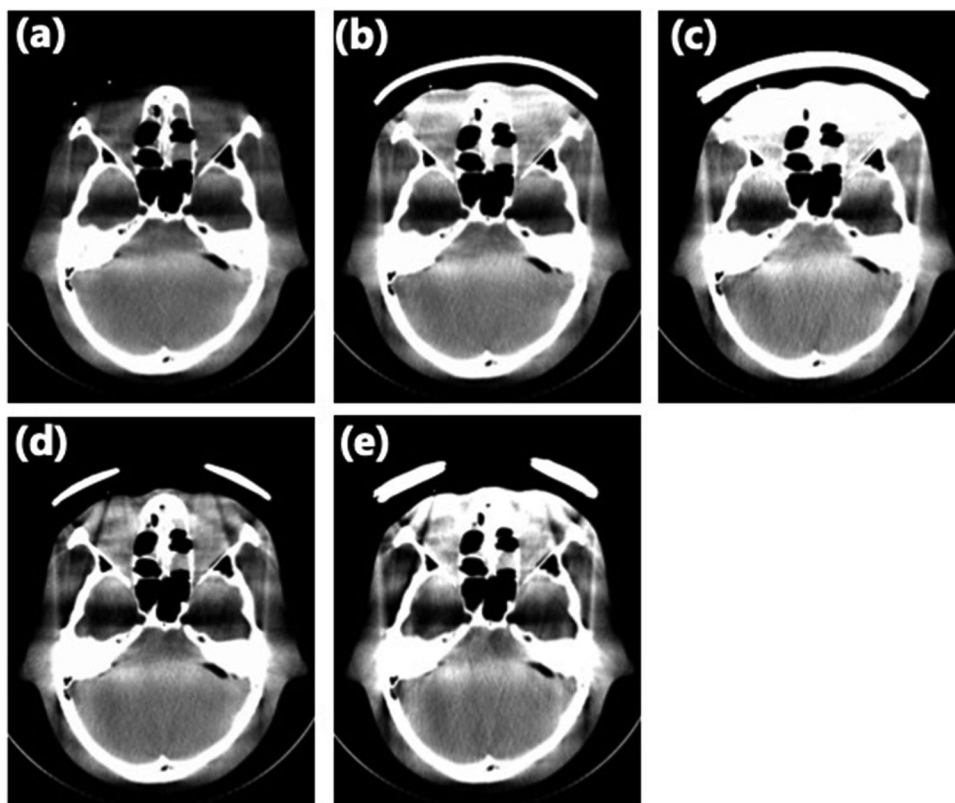


Fig. 12 Δ PVs for the different number of bismuth shield for each region of interest. Error bars represent the standard deviation of Δ PV

distance of the bismuth shield was far from the surface of the head phantom. Furthermore, the incidence of backscattered X-rays to the lenses was affected by the interaction between the X-rays incident from the back of the head phantom and the bismuth shield.

Placement distances of 0 or 5 mm were unsuitable, because the distance to the surface of the subject was very close, resulting in a decrease in image quality, and a placement distance of 20 mm was not effective in reducing the

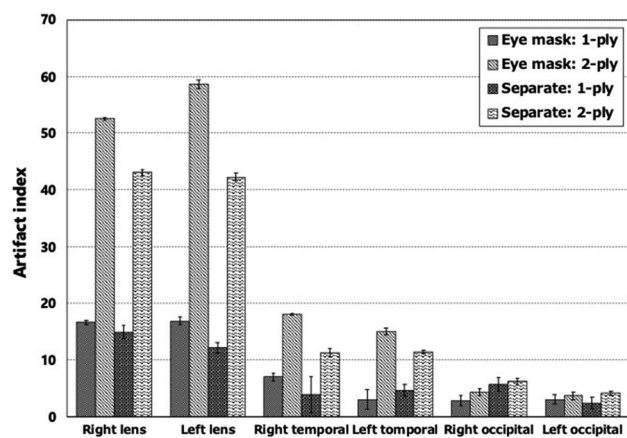


Fig. 13 Artifact indices for the different numbers of the bismuth shield for each region of interest. Error bars represent the standard deviation of the artifact index

lens doses. Therefore, considering the balance between the dose reduction rate and the image quality, the optimum placement distance was considered as 10 mm. However, there is a possibility that the optimum distance would vary if different systems, conditions, and types of bismuth shields are used.

Wang et al. evaluated the lens doses and image quality as noise and CT number with bismuth shield at different

Table 4 Lens doses and lens dose reduction rates for different positions of “bismuth shield: separate”

	Lens dose [mGy]			Dose reduction rate [%]		
	Right lens	Left lens	Average	Right lens	Left lens	Average
Reference	30.6 ± 0.12	31.2 ± 0.14	30.9 ± 0.11	–	–	–
Inside	31.2 ± 0.12	31.7 ± 0.36	31.4 ± 0.24	– 1.9 ± 0.57	– 1.6 ± 1.24	– 1.8 ± 0.86
Middle	26.3 ± 0.19	26.3 ± 0.12	26.3 ± 0.15	13.8 ± 0.70	15.7 ± 0.54	14.8 ± 0.58
Outside	22.5 ± 0.08	22.7 ± 0.07	22.8 ± 0.07	26.4 ± 0.39	27.4 ± 0.40	26.9 ± 0.36

The distance between the bismuth shield and the surface of the eyes was 10 mm. Data are presented as mean ± standard deviation

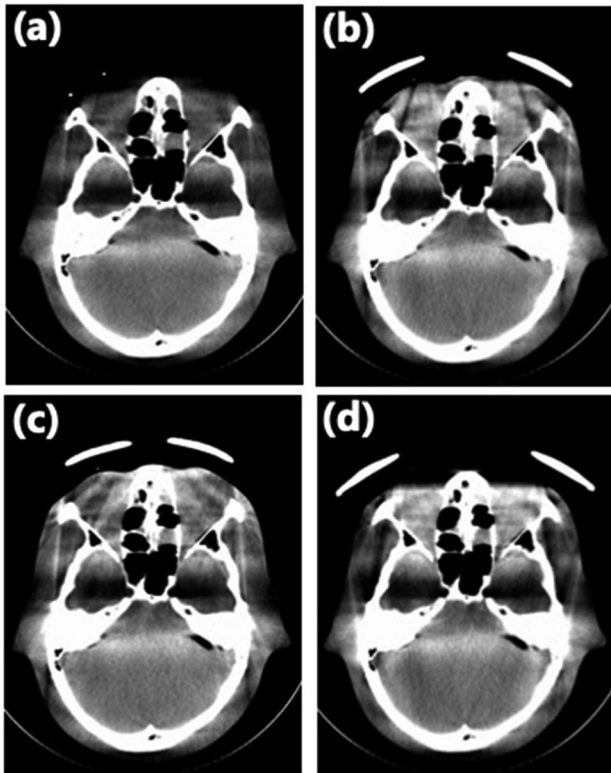


Fig. 14 Images of head phantom for different positions of bismuth shields. **a** Reference, **b** middle, **c** inside, and **d** outside.

distances (0, 2, 3, and 4 cm) from the phantom surface in head CT [31]. Even though the lens doses increased by increasing the distance of the bismuth shield, the image quality improved significantly, which is consistent with the results of this study.

4.2 Lens dose measurement and image quality assessment with different numbers of bismuth shields

To investigate the effect of the number of bismuth shields on the lens dose reduction rates and image quality, “bismuth shield: eye mask” and “bismuth shield: separate” were used. When the number of bismuth shields was changed from

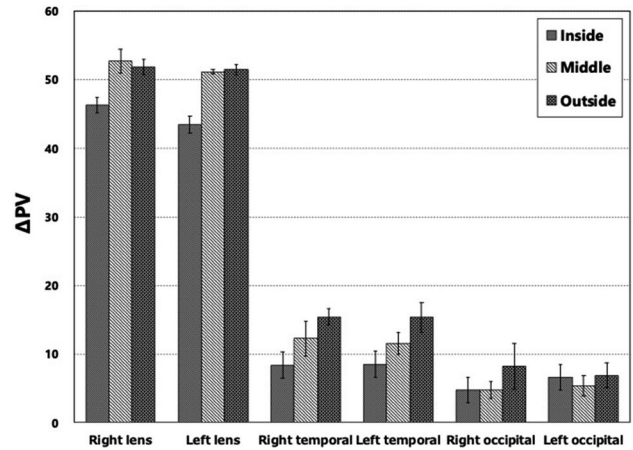


Fig. 15 ΔPVs for the different positions of “bismuth shield: separate” for each region of interest. Error bars represent the standard deviation of ΔPV

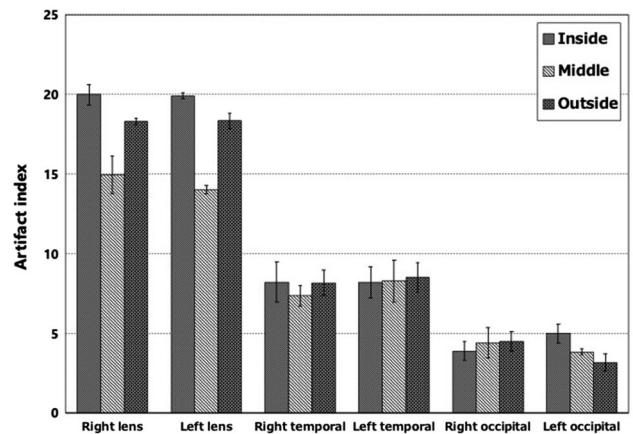


Fig. 16 Artifact indices for the different positions of “bismuth shield: separate” for each region of interest. Error bars represent the standard deviation of the artifact index

1-ply to 2-ply, the lens dose reduction rate was improved in both bismuth shields. However, the ΔPVs and AIs of the CBCT image, especially in the right and left lens regions near the placements of the bismuth shield, also increased.

Wang et al. evaluated the lens dose reduction rate and image quality using 1-ply and 2-ply bismuth shields for head CT [31]. In this study, the dose reduction rate improved from 38 to 79% by increasing the number of bismuth shields, but it was concluded that this method is not practical, because it generates streak artifacts and increases the CT number and image noise in front of the head phantom. The report shows similar results to those of the present study, although the rotation method of the X-ray tube differed between the head CT and CBCT scans. As a result, increasing the number of bismuth shields is undesirable from the perspective of the image quality of CBCT. Although this is a subjective judgement, the authors of this study believe that the use of 1-ply bismuth shields is more suitable.

4.3 Lens dose measurement and image quality assessment with a change of position

The authors also evaluated the effect of changes in the position of the bismuth shields on the lens dose reduction rate and image quality. By changing the position of the bismuth shield, dividing it into internal, middle, and external, the dose reduction rate was improved by placing it externally.

The average dose reduction rates were $-1.8 \pm 0.86\%$, $14.8 \pm 0.58\%$, and $26.9 \pm 0.36\%$ when the bismuth shield was placed internally, in the middle, and externally, respectively. When the bismuth shield was placed inside, the lens dose was larger. This is because there was almost no shielding effect of the primary X-rays owing to the change in the position of the bismuth shield. The lens dose increased owing to the effect of the backscattered radiation caused by the interaction between the X-rays incident from the back of the head phantom and the bismuth shield. The dose reduction rate was substantially improved by placing the bismuth shield on the outside of the phantom, because the bismuth shield was placed to match the X-ray tube rotation orbit, which rotated the arc from left anterior oblique 120° to right anterior oblique 120° around the posterior side.

The Δ PVs of the lens and temporal region were reduced by placing the bismuth shield inside. By placing the bismuth shield on the outside, the Δ PVs of the temporal region increased slightly, and the AIs of the lens increased. CBCT imaging is used to evaluate intracranial lesions, such as brain parenchyma or aneurysms, and lenses are rarely observed. Placing the bismuth shield outside the lens may cause some degradation in image quality, but it is unlikely to be a clinical disadvantage. Therefore, considering the significant improvement in the dose reduction rate at the cost of slightly reduced image quality, we believe that placing the bismuth shield on the outside is useful for lens protection during CBCT imaging.

4.4 Significance of lens protection in CBCT

In this study, we evaluated the distance, number, and position of bismuth shields in CBCT imaging. It was found that the optimum placement conditions of the bismuth shield are as follows: distance of 10 mm from the head phantom surface, number of sheets as 1-ply, and the placement position was outside. The average dose reduction rate was $26.9 \pm 0.36\%$ when the CBCT scan was performed under the optimal placement condition. The optimum bismuth shield placement distance and the number of placements, as revealed in this study, were similar to those reported in the previous studies on head CT scans [30, 31]. Regarding the dose reduction rates, the results of CBCT were lower than those of head CT [22, 25–27, 29, 31]. This is because the rotation orbits of the X-ray tube between CBCT and CT were different. In CBCT, although the amount of primary X-rays incident from the front of the subject is less than that in CT, a certain number of primary X-rays are incident on the eye lens; therefore, using a bismuth shield to protect the lens is recommended.

With the use of protective materials, streak artifacts occur mainly in the portion of the eye directly under the materials, such as the anterior part of the CBCT image. This streak artifact interferes with the evaluation of intracranial lesions (cerebral hemorrhage and cerebral infarction). Although it was clarified that strong artifacts occurred near the patient's eye under the optimized bismuth shield placement conditions in this study, the effect on the temporal and occipital lobes was small. However, the observation site and the artifact occurrence site have a close positional relationship in the case of coil embolization for an anterior communicating artery aneurysm or anterior cerebral aneurysm near the eyes and embolization for dural arteriovenous fistula in the cavernous sinus. Therefore, it is necessary to pay sufficient attention to the use of protective materials. In contrast, for cases of coil embolization of vertebral or basilar artery aneurysms or embolization of cerebral arteriovenous malformations in the occipital or parietal lobes, the area observed and the area where artifacts are generated are far apart. Thus, the effect on clinical images may be reduced. In such cases, it is considered that the lens dose reduction rate may be further improved using a bismuth shield or placing the bismuth shield closer to the subject surface.

In this study, lens dose reduction was performed specifically for CBCT imaging, but it is necessary to consider lens protection during cerebral angiography for diagnosis and INR in the future. Kim et al. reported that they reduced the radiation dose while maintaining image quality using an imaging protocol in which the focal spot was changed from a large focus to a small focus during DSA imaging [44]. Thus, for other procedures such as DSA imaging, it is necessary to take measures to further reduce the radiation dose, such as

collimation of the radiation field to the eyes, control of the pulse rate of fluoroscopy, and frame number.

The criteria for AI of proper CBCT images when using bismuth shields were not presented in this study, but they need to be clarified in further studies.

5 Conclusion

This study was performed to determine the placement distance, number, and position of the bismuth shield for the development of a lens protective device for CBCT. Considering the lens dose reduction rate and image quality, the bismuth shield was placed 10 mm from the surface of the subject, the number of bismuth shields used was 1-ply, and the placement position was outside. When the optimum bismuth shield placement conditions were used, the lens dose reduction rate was $26.9 \pm 0.36\%$ (right–left average).

Acknowledgements This study was supported by JSPS KAKENHI Grant No: JP19K17183. This study was partly supported by a research award grant from the Japanese Society of Radiological Technology, Tokyo branch.

Declarations

Conflict of interest The authors declare that they have no conflict of interest.

Research involving human participants This article does not contain any studies with human participants.

Research involving animals This article does not contain any studies involving animals.

References

- Chida K, Inaba Y, Saito H, Ishibashi T, Takahashi S, Kohzuki M, et al. Radiation dose of interventional radiology system using a flat-panel detector. *Am J Roentgenol*. 2009;193:1680–5.
- Chida K, Kaga Y, Haga Y, Kataoka N, Kumasaka E, Meguro T, et al. Occupational dose in interventional radiology procedures. *Am J Roentgenol*. 2013;200:138–41.
- Chida K, Ohno T, Kakizaki S, Takegawa M, Yuuki H, Nakada M, et al. Radiation dose to the pediatric cardiac catheterization and intervention patient. *Am J Roentgenol*. 2010;195:1175–9.
- Chida K, Saito H, Otani H, Kohzuki M, Takahashi S, Yamada S, et al. Relationship between fluoroscopic time, dose-area product, body weight, and maximum radiation skin dose in cardiac interventional procedures. *Am J Roentgenol*. 2006;186:774–8.
- Chida K, Takahashi T, Ito D, Shimura H, Takeda K, Zuguchi M. Clarifying and visualizing sources of staff-received scattered radiation in interventional procedures. *Am J Roentgenol*. 2011;197:W900–3.
- Ishii H, Chida K, Satsurai K, Haga Y, Kaga Y, Abe M, et al. A phantom study to determine the optimal placement of eye dose-meters on interventional cardiology staff. *Radiat Prot Dosimetry*. 2019;185:409–13.
- Kawauchi S, Moritake T, Hayakawa M, Hamada Y, Sakuma H, Yoda S, et al. Estimation of maximum entrance skin dose during cerebral angiography. *Nihon Hoshasen Gijutsu Gakkai Zasshi* (in Japanese). 2015;71:746–57.
- Matsunaga Y, Chida K, Kondo Y, Kobayashi K, Kobayashi M, Minami K, et al. Diagnostic reference levels and achievable doses for common computed tomography examinations: results from the Japanese nationwide dose survey. *Br J Radiol*. 2019;92:20180290.
- Moritake T, Hayakawa M, Matsumaru Y, Takigawa T, Koguchi Y, Miyamoto Y, et al. Precise mapping system of entrance skin dose during endovascular embolization for cerebral aneurysm. *Radiat Meas*. 2011;46:2103–6.
- Sánchez RM, Vañó E, Fernández JM, Rosati S, López-Ibor L. Radiation doses in patient eye lenses during interventional neuro-radiology procedures. *AJNR Am J Neuroradiol*. 2016;37:402–7.
- Kawauchi S, Chida K, Moritake T, Matsumaru Y, Hamada Y, Sakuma H, et al. Estimation of patient lens dose associated with C-arm cone-beam computed tomography usage during interventional neuroradiology. *Radiat Prot Dosimetry*. 2019;184:138–47.
- Irie K, Murayama Y, Saguchi T, Ishibashi T, Ebara M, Takao H, et al. Dynact soft-tissue visualization using an angiographic C-arm system: initial clinical experience in the operating room. *Neurosurgery*. 2008;62:266–72.
- Kanayama S, Hara T, Hamada Y, Matsumaru Y. Potential of 80-kV high-resolution cone-beam CT imaging combined with an optimized protocol for neurological surgery. *Neuroradiology*. 2015;57:155–62.
- Struffert T, Richter G, Engelhorn T, Doelken M, Goelitz P, Kalender WA, et al. Visualisation of intracerebral haemorrhage with flat-detector CT compared to multislice CT: results in 44 cases. *Eur Radiol*. 2009;19:619–25.
- Tsuruta W, Matsumaru Y, Hamada Y, Hayakawa M, Kamiya Y. Analysis of closed-cell intracranial stent characteristics using cone-beam computed tomography with contrast material. *Neurol Med Chir (Tokyo)*. 2013;53:403–8.
- Stewart FA, Akleyev AV, Hauer-Jensen M, Hendry JH, Kleiman NJ, MacVittie TJ, Aleman BM, Edgar AB, Mabuchi K, Muirhead CR, Shore RE, Wallace WH. ICRP publication 118: ICRP statement on tissue reactions and early and late effects of radiation in normal tissues and organs-threshold doses for tissue reactions in a radiation protection context. *Ann ICRP*. 2012;41:1–322.
- Endo M, Haga Y, Sota M, Tanaka A, Otomo K, Murabayashi Y, et al. Evaluation of novel X-ray protective eyewear in reducing the eye dose to interventional radiology physicians. *J Radiat Res*. 2021;62:414–9.
- Haga Y, Chida K, Kaga Y, Sota M, Meguro T, Zuguchi M. Occupational eye dose in interventional cardiology procedures. *Sci Rep*. 2017;7:569.
- Kato M, Chida K, Ishida T, Toyoshima H, Yoshida Y, Yoshioka S, et al. Occupational radiation exposure of the eye in neurovascular interventional physician. *Radiat Prot Dosimetry*. 2019;185:151–6.
- Wang C, Nguyen G, Toncheva G, Jiang X, Ferrell A, Smith T, et al. Evaluation of patient effective dose of neurovascular imaging protocols for C-arm cone-beam CT. *AJR Am J Roentgenol*. 2014;202:1072–7.
- Kawauchi S, Chida K, Moritake T, Hamada Y, Matsumaru Y, Tsuruta W, et al. Treatment of internal carotid aneurysms using pipeline embolization devices: measuring the radiation dose of the patient and determining the factors affecting it. *Radiat Prot Dosimetry*. 2020;3:389.
- Ciarmatori A, Nocetti L, Mistretta G, Zambelli G, Costi T. Reducing absorbed dose to eye lenses in head CT examinations: the effect of bismuth shielding. *Australas Phys Eng Sci Med*. 2016;39:583–9.

23. Colletti PM, Micheli OA, Lee KH. To shield or not to shield: application of bismuth breast shields. *Am J Roentgenol*. 2013;200:503–7.
24. Hopper KD. Orbital, thyroid, and breast superficial radiation shielding for patients undergoing diagnostic CT. *Semin Ultrasound CT MR*. 2002;23:423–7.
25. Hopper KD, Neuman JD, King SH, Kunselman AR. Radioprotection to the eye during CT scanning. *AJNR Am J Neuroradiol*. 2001;22:1194–8.
26. Kim JS, Kwon SM, Kim JM, Yoon SW. New organ-based tube current modulation method to reduce the radiation dose during computed tomography of the head: evaluation of image quality and radiation dose to the eyes in the phantom study. *Radiol Med*. 2017;122:601–8.
27. McLaughlin DJ, Mooney RB. Dose reduction to radiosensitive tissues in CT. Do commercially available shields meet the users' needs? *Clin Radiol*. 2004;59:446–50.
28. Mehnati P, Malekzadeh R, Sooteh MY. Use of bismuth shield for protection of superficial radiosensitive organs in patients undergoing computed tomography: a literature review and meta-analysis. *Radiol Phys Technol*. 2019;12:6–25.
29. Nikupaavo U, Kaasalainen T, Reijonen V, Ahonen SM, Kortensniemi M. Lens dose in routine head CT: comparison of different optimization methods with anthropomorphic phantoms. *Am J Roentgenol*. 2015;204:117–23.
30. Raissaki M, Perisinakis K, Damlakis J, Gourtsoyiannis N. Eye-lens bismuth shielding in paediatric head CT: artefact evaluation and reduction. *Pediatr Radiol*. 2010;40:1748–54.
31. Wang J, Duan X, Christner JA, Leng S, Grant KL, McCollough CH. Bismuth shielding, organ-based tube current modulation, and global reduction of tube current for dose reduction to the eye at head CT. *Radiology*. 2012;262:191–8.
32. Kawauchi S, Chida K, Moritake T, Hamada Y, Tsuruta W. Radioprotection of eye lens using protective material in neuro cone-beam computed tomography: Estimation of dose reduction rate and image quality. *Phys Med*. 2021;82:192–9.
33. Liao YL, Lai NK, Tyan YS, Tsai HY. Bismuth shield affecting CT image quality and radiation dose in adjacent and distant zones relative to shielding surface: a phantom study. *Biomed J*. 2019;42:343–51.
34. Chida K, Kato M, Inaba Y, Kobayashi R, Nakamura M, Abe Y, et al. Real-time patient radiation dosimeter for use in interventional radiology. *Phys Med*. 2016;32:1475–8.
35. Inaba Y, Chida K, Murabayashi Y, Endo M, Otomo K, Zuguchi M. An initial investigation of a wireless patient radiation dosimeter for use in interventional radiology. *Radiol Phys Technol*. 2020;13:321–6.
36. Inaba Y, Nakamura M, Chida K, Zuguchi M. Effectiveness of a novel real-time dosimeter in interventional radiology: a comparison of new and old radiation sensors. *Radiol Phys Technol*. 2018;11:445–50.
37. Inaba Y, Nakamura M, Zuguchi M, Chida K. Development of novel real-time radiation systems using 4-channel sensors. *Sensors (Basel)*. 2020;20:2741.
38. Kato M, Chida K, Nakamura M, Toyoshima H, Terata K, Abe Y. New real-time patient radiation dosimeter for use in radiofrequency catheter ablation. *J Radiat Res*. 2019;60:215–20.
39. Nakamura M, Chida K, Zuguchi M. Red emission phosphor for real-time skin dosimeter for fluoroscopy and interventional radiology. *Med Phys*. 2014;41:101913.
40. Nakamura M, Chida K, Zuguchi M. Novel dosimeter using a non-toxic phosphor for real-time monitoring of patient radiation dose in interventional radiology. *Am J Roentgenol*. 2015;205:W202–6.
41. Dong Y, Shi AJ, Wu JL, Wang RX, Sun LF, Liu AL, et al. Metal artifact reduction using virtual monochromatic images for patients with pedicle screws implants on CT. *Eur Spine J*. 2016;25:1754–63.
42. Kuya K, Shinohara Y, Kato A, Sakamoto M, Kurosaki M, Ogawa T. Reduction of metal artifacts due to dental hardware in computed tomography angiography: assessment of the utility of model-based iterative reconstruction. *Neuroradiology*. 2017;59:231–5.
43. Lin XZ, Miao F, Li JY, Dong HP, Shen Y, Chen KM. High-definition CT Gemstone spectral imaging of the brain: initial results of selecting optimal monochromatic image for beam-hardening artifacts and image noise reduction. *J Comput Assist Tomogr*. 2011;35:294–7.
44. Kim DJ, Park MK, Jung DE, Kang JH, Kim BM. Radiation dose reduction without compromise to image quality by alterations of filtration and focal spot size in cerebral angiography. *Korean J Radiol*. 2017;18:722–8.

Publisher's Note Springer Nature remains neutral with regard to jurisdictional claims in published maps and institutional affiliations.